

JAC conceptual (final) design document

Masayuki Nakano

December 6, 2024

Contents

| | |
|--|-----------|
| 1 Relevant document | 3 |
| 2 Overview | 4 |
| 2.1 Background and Motivation | 4 |
| 2.2 Block Diagram | 4 |
| 2.3 Requirements | 5 |
| 3 JAC Design Considerations | 5 |
| 3.1 Jitter attenuation | 5 |
| 3.1.1 Jitter Expression | 5 |
| 3.1.2 Output jitter estimation | 7 |
| 3.2 JAC design candidate | 8 |
| 3.2.1 Jitter attenuation | 8 |
| 3.2.2 Polarization separation | 8 |
| 3.2.3 RF filtering | 12 |
| 3.2.4 Higher-order mode filtering | 12 |
| 3.3 Conclusion | 12 |
| 3.4 Specification of the aLIGO PMC | 13 |
| 4 HAM1 layout | 13 |
| 4.1 Overview | 13 |
| 4.2 Seismic Isolation | 13 |
| 4.3 Mode matching | 13 |
| 4.3.1 Requirement for the mode mismatching | 18 |
| 4.3.2 PSL to JAC | 18 |
| 4.3.3 JAC to IMC | 21 |
| 4.4 Thermal Lens of the EOM | 21 |
| 4.5 Height adjustment | 24 |
| 4.6 Viewport | 25 |
| 4.7 Power adjustment | 25 |
| 4.8 Leakage port | 25 |

| | |
|--|-----------|
| 5 JAC Control Loop Design | 28 |
| 5.1 Length Control | 28 |
| 5.1.1 Modulation | 28 |
| 5.1.2 Sensor | 28 |
| 5.1.3 Actuator | 29 |
| 5.1.4 Servo | 29 |
| 5.1.5 Length fluctuation | 31 |
| 5.1.6 Intensity noise due to residual length fluctuation | 31 |
| 5.1.7 Phase noise due to residual length fluctuation | 31 |
| 5.1.8 Slow control | 36 |
| 5.1.9 Conclusion of the length control | 37 |
| 5.2 Alignment control | 37 |
| 6 In air table layout | 37 |
| 6.1 Layout | 37 |
| 6.2 Gouy phase telescope | 38 |
| 6.3 High power beam dump | 38 |
| 6.4 ALS Path | 39 |
| 7 Risk Registry | 39 |
| 7.1 JM misalignment | 39 |
| 8 Open questions | 42 |
| 8.1 Thermal effect of the JAC | 42 |
| 8.2 Length fluctuation | 43 |
| 8.3 Stray light control | 43 |
| 9 Safety | 43 |
| 9.1 Laser safety | 43 |
| 10 Wiring | 44 |
| 10.1 Analog circuit | 44 |
| 10.2 CDS | 44 |
| 10.3 HAM1 flange feedthrough | 44 |
| 11 Vacuum compatibility | 44 |
| 11.1 Cavity | 44 |
| 11.2 Electronics | 44 |
| 12 Test plan | 44 |
| 12.1 Jitter attenuation | 45 |
| 13 Installation plan | 45 |
| 14 | 45 |

1 Relavant document

Jitter Attenuation Cavity(JAC)

- [T2400329](#) Jitter Attenuation Cavity document tree
- [E2400349](#) Jitter Attenuation Cavity Design Requirements Document
- [G2401650](#) Jitter Attenuation Cavity preliminary design report
- [L2400050](#) JAC weekly meeting note
- [D2400257](#) Schematic wiring diagram of JAC for O5
- [parts list](#)
- [T2400328](#) JAC optics list
- [T2400360](#) List of relevant circuits for the JAC

Pre-Mode Cleaner (PMC)

- [E1200491](#) aLIGO Pre-mode cleaner document tree
-

Others

- [E2400246](#): A+ EOM crystal thermal lensing test

Drawing package

- [D1600270](#): aLIGO, PSL, PreMode Cleaner, SPACER ASSY.

Interface control document

Laser noise requirement

- [T0900649](#) PSL final design document

HAM1 ISI

- [E2200105](#): HAM1 stack to HAM1-ISI: E2200105

Optical path

- [HAM1 optical path](#)
- [T2400151](#): PSL+ Preliminary Table Layout Investigation
- [E1300206](#): aLIGO HAM2 Layout for IO Auxiliary Optics
- [T2400151](#): PSL+ Preliminary Table Layout Investigation
- [D1201103](#): ISCT1 Optical Layout

Wiring

- [D1900511](#): O5 ISC/SQZ Wiring Diagram for Corner Station
- [D0902810](#): aLIGO SUS HAM 1-2 System Wiring Diagrams
- [D1900511](#): O5 ISC/SQZ Wiring Diagram for Corner Station
- [D1002704](#): Rack and Cable Tray Layout_LVEA_H1
- [G1400098](#): Rack and Cable Tray Layout_LVEA_L1
- [D1201121](#): LVEA Rack PSL-R2
- [D1001460](#): ISC R1
- [D1001425](#): ISC R2
- [D1001427](#): ISC C1-C4 (CER Rack Layout)
- [E1100591](#): RF Signal Distribution (Cabling)

Viewport and flange

- [T2300221](#): Post-O4 HAM1 Flange Layout Discussions
- [D1101714](#): ALIGO HIGH POWER WEDGED 6IN VIEWPORT ASSY

2 Overview

2.1 Background and Motivation

During the O4 run, input beam jitter was identified as one of the noise sources limiting sensitivity. Jitter-induced noise was observed to impact sensitivity at both the LLO and LHO sites in the 100 Hz to 1 kHz range, as shown in Fig. ???. As sensitivity improves for the upcoming O5 observation, this noise is expected to further limit performance. It was determined that beam jitter is introduced by the PSL periscope. To mitigate this, an optical cavity, called the Jitter Attenuation Cavity (JAC), has been proposed to be installed between the PSL and the IMC. The purpose of the JAC is to filter out the first-order TEM mode, thereby reducing jitter noise. The installation of the JAC is planned for the O5 observation period.

2.2 Block Diagram

The Jitter Attenuation Cavity (JAC) is located between the PSL and the IMC, in the HAM1 chamber. The output beam from the PSL passes through the JAC and is then directed to the IMC. The reflected beam is directed out of the HAM1 chamber to the ISCT1 and is used for length and alignment control.

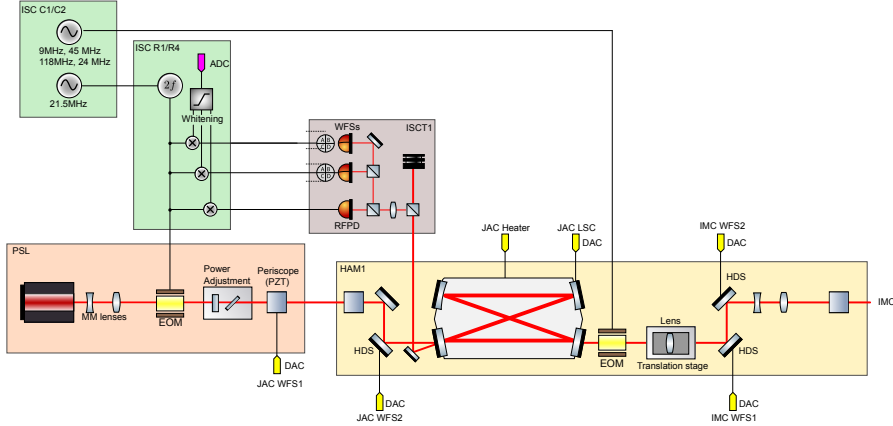


Figure 1: JAC block diagram.

2.3 Requirements

The jitter attenuation requirement for the JAC is set at 30 dB. This level ensures that the jitter noise projection to the gravitational wave sensitivity is lower than the A+ target sensitivity by a factor of 10, assuming the same input jitter and jitter coupling as observed in O4.

3 JAC Design Considerations

3.1 Jitter attenuation

In this section, we will show three JAC designs and discuss their jitter attenuation performance.

3.1.1 Jitter Expression

Before discussing the JAC geometry, we describe the beam jitter mathematically. Assuming our laser is traveling along the z-axis and is in the fundamental transverse electromagnetic mode (TEM00). For simplicity, we consider only the xz-plane. The finite beam shift in the x-direction Δx and the tilt around the beam waist $\Delta\theta$ can be described as a conversion from TEM00 to TEM10 mode [?]:

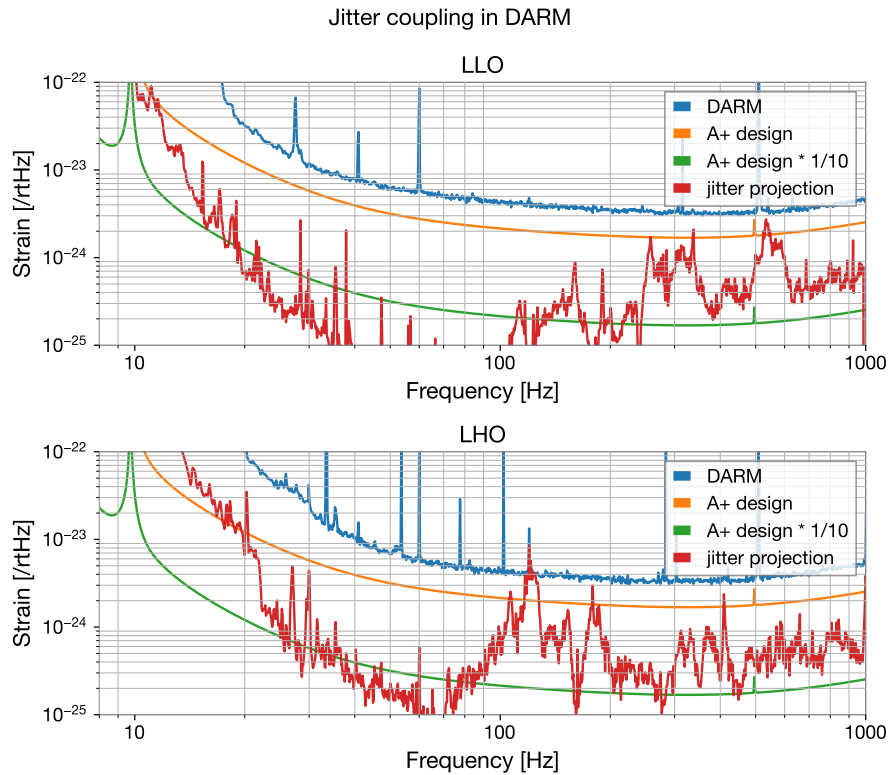


Figure 2: Jitter noise projection to DARM sensitivity. The orange trace shows the target A+ sensitivity, and the green trace represents the jitter noise attenuation requirement, which is 10 times lower than the A+ target sensitivity.

$$E' = E_0 \left(\left(1 - \left(\frac{\Delta x}{w_0} \right)^2 - \left(\frac{\Delta \theta}{\alpha} \right)^2 \right) e_0 + \left(\frac{\Delta x}{w_0} + i \frac{\Delta \theta}{\alpha} \right) e_1 \right), \quad (1)$$

where E' is the electric field of shifted beam, E_0 is the input electric field amplitude, w_0 and α are the waist size and the divergence angle of the beam, and e_0 and e_1 are the intensity distributions of the TEM00 and TEM10 modes, respectively.

As discussed above, the beam jitter can be described as intensity fluctuations in the TEM10/TEM01 modes. Therefore, by filtering out these modes using the JAC, the jitter noise can be attenuated. The jitter attenuation performance of the JAC is evaluated by the attenuation gain of the TEM10/01 modes.

For the following discussion, we describe the first-order modes generated by mirror motion located at a distance z from the beam waist. The motion of the mirror by $\Delta\theta$ moves the waist by $z\Delta\theta$ and tilts the beam by $\Delta\theta$ around the beam waist. Thus, the TEM10 amplitude generated by this mirror motion is

$$A_1 = \sqrt{\left(\frac{z\Delta\theta}{w_0} \right)^2 + \left(\frac{\Delta\theta}{\alpha} \right)^2} = \frac{kw_0}{\cos \eta(z)} \Delta\theta, \quad (2)$$

where k is the wavenumber and $\eta(z)$ is the Gouy phase at position z .

3.1.2 Output jitter estimation

In this subsection, we describe how the jitter noise is estimated in following. The jitter included in the JAC output is the sum of the residual jitter determined by the first-order TEM mode filtering efficiency of the JAC and the jitter present in the incident light, and the jitter introduced by the JAC's motion.

We start from considering the residual jitter at the JAC output. From the jitter noise evaluation in O4, it has been found that the jitter included in the incident light is mostly introduced by the upper mirror of the PSL periscope across the entire band. The periscope mirror motion is estimated by the IMC WFS signals as witness, calibrated by the PZT injection measurement [?]. Once the JAC geometry is determined, the waist size and the Gouy phase at the PSL periscope are determined. Here, the mode matching to the JAC is assumed to be done in the PSL. Then, the first-order TEM mode can be calculated by using equation (2). Since the jitter attenuation gain is also determined by the JAC geometry and the finesse, the output residual jitter can be estimated.

Then, the introduced jitter by the JAC motion is also estimated. The JAC is assumed to be located on the ISI table newly installed into the HAM1 chamber. (The discussion on the seismic isolation requirement will be discussed in the following section.) The introduced jitter can be calculated by the ISI motion and the cavity parameters of the JAC.

3.2 JAC design candidate

Along with the discussion so far, the output beam jitter is estimated with three different configurations. The key parameters of each candidate are listed in Table 1.

We have two choices regarding the cavity configuration: triangular and bow-tie. The size of the cavity is chosen to be similar to the aLIGO PMC. In fact, we have a couple of spare PMCs, so an exact replication of the current PMC design is one candidate. Additionally, it is feasible to replace the mirrors of the PMC without altering its body, so a bow-tie cavity with mirrors of different radii of curvature (RoC) was considered as another candidate. The RoC is chosen based on the Gouy phase and the overlap with higher-order modes.

For the triangular cavity, a dimension similar to the PMC is selected. The RoC is chosen in the same way as for the bow-tie cavity. The finesse is determined such that the power density on the mirrors remains below 1 MW/cm² with 100W input.

3.2.1 Jitter attenuation

and the expected jitter attenuation performance is shown in Fig. 3. The newly designed cavities have larger waist sizes compared to the PMC, and a higher finesse is achievable, which results in the higher jitter attenuation. When comparing the newly designed triangular and bow-tie cavities, the mirrors in the bow-tie cavity are located farther from the waist, resulting in a larger beam size and higher finesse capability. This gives the bow-tie cavity the highest attenuation gain among the three configurations. However, all three configurations meet the requirements for jitter attenuation.

3.2.2 Polarization separation

It is important to note that odd-mirror cavities, such as the triangular design, have separated resonances for each polarization. In contrast, even-mirror cavities, like the bow-tie design, have resonant frequencies within the cavity linewidth. When the mix-polarized beam is injected, due to this multi-resonant condition, the error signal of the cavity locking will have an offset, and this offset will detune the cavity. A cavity detuned from resonance will convert the residual error between the resonant frequency and the laser frequency into intensity fluctuations. From this perspective, the triangular cavity offers an advantage over the bow-tie cavity. In this section, we will calculate this effect for the design evaluation.

By assuming the JAC is critically coupled, the transmission power can be written as

$$P_T(\hat{\omega}) = \frac{P}{1 + (\hat{\omega} - \hat{\omega}_0)^2} \equiv PL(\hat{\omega} - \hat{\omega}_0), \quad (3)$$

where $L(\hat{\omega})$ is the Lorentzian function, P is the laser power, $\hat{\omega}$ is the normalized angular frequency by the linewidth $\omega_c = \omega_{\text{FSR}}/2\mathcal{F}$, and $\hat{\omega}_0$ is the normalized

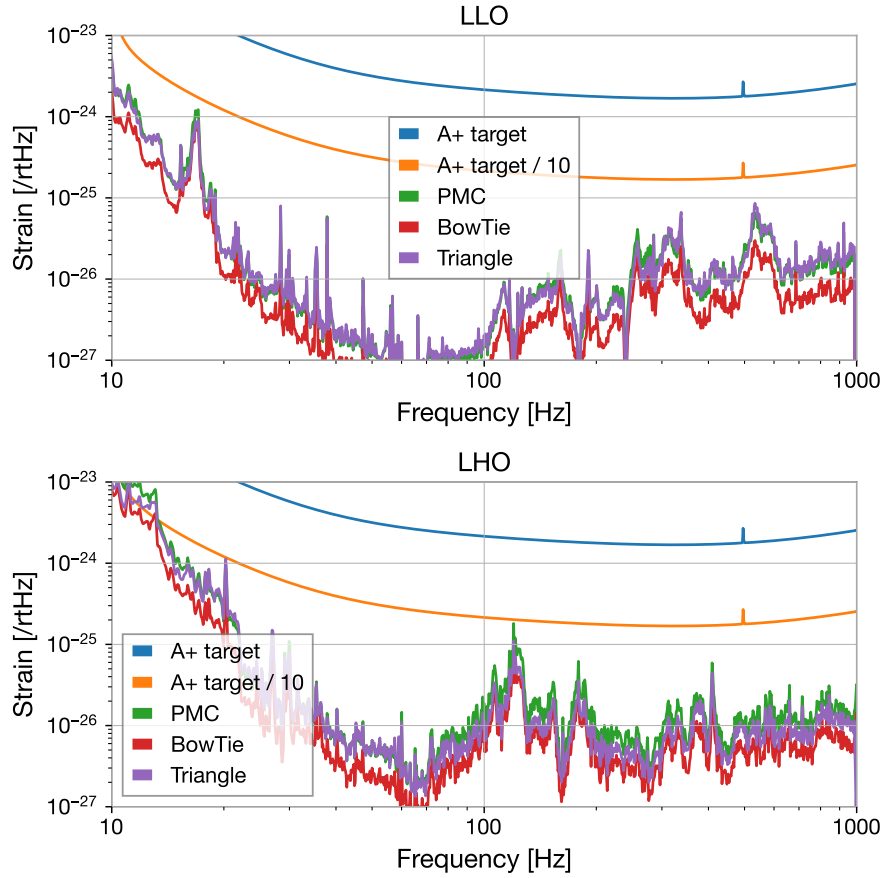


Figure 3: Projected jitter noise with three JAC design candidate. PMC is exactly same design with the current aLIGO PMC, and bow-tie and triangle cavity are newly designed ones. All three configuration attenuate the jitter noise below the 10 times below of the A+ target sensitivity, and meet the requirement for the jitter attenuation

resonant frequency of the cavity. Let's assume the resonant frequency for each polarization has a shift of $\Delta\hat{\omega}$. If the injected beam is not perfectly polarized and has an angle of θ from s-pol, then the transmission power from the cavity will be

$$\begin{aligned} P_T &= P \cos^2 \theta L(\hat{\omega} - \hat{\omega}_0) + P \sin^2 \theta L(\hat{\omega} - (\hat{\omega}_0 + \Delta\hat{\omega})) \\ &\simeq P \left(L(\hat{\omega} - \hat{\omega}_0) + \frac{dL}{d\hat{\omega}}(\hat{\omega} - \hat{\omega}_0) \Delta\hat{\omega} \sin^2 \theta \right) \\ &\simeq PL(\hat{\omega} - (\hat{\omega}_0 - \Delta\hat{\omega} \sin^2 \theta)). \end{aligned} \quad (4)$$

Therefore, the peak position of the resonance will shift by $\Delta\hat{\omega} \sin^2 \theta$. Practically, we will tweak the locking point to maximize the transmission power, so with mixed polarization, the cavity will be detuned by this amount. Then, the derivative of the output power can be written as

$$\frac{dP_T}{d\hat{\omega}} = \frac{2P(\hat{\omega} - \hat{\omega}_0)}{1 + (\hat{\omega} - \hat{\omega}_0)^2}. \quad (5)$$

This value can be considered as the transfer function from the frequency fluctuation, or more precisely the residual error between the laser frequency and the JAC resonant frequency, to the relative intensity noise of the cavity. Thus, the transfer function of the detuned cavity due to mis-polarization can be written as

$$\frac{dP}{d\hat{\omega}}(\theta) = \frac{2\Delta\hat{\omega} \sin^2 \theta}{1 + (\Delta\hat{\omega} \sin^2 \theta)^2} \simeq 2\Delta\hat{\omega}\theta^2. \quad (6)$$

By converting the unit from the normalized frequency to the length fluctuation, the transfer function from the length fluctuation to the relative intensity noise of the output beam can be calculated as

$$\begin{aligned} \frac{dP}{dl}(\theta) &= \frac{dP}{d\hat{\omega}}(\theta) \times \frac{\hat{\omega}}{l} = 2\Delta\hat{\omega}\theta^2 \times \frac{4\mathcal{F}}{\lambda} \\ &= 2.9 \times 10^{-5} / \text{nm} \times \left(\frac{\Delta\hat{\omega}}{0.1} \right) \times \left(\frac{\mathcal{F}}{125} \right) \times \left(\frac{1064 \text{ nm}}{\lambda} \right) \times \left(\frac{\theta}{1 \text{ deg}} \right)^2. \end{aligned} \quad (7)$$

This model was also double-checked with finesse [?], and the calculated transfer function agrees with the finesse calculation as shown in Fig.4

The resonant frequency shift for the PMC is reported as one-tenth of the cavity linewidth [?]. The estimated residual length fluctuation is 10^{-5} to 10^{-4} nm in the observation range as described in Sec.5.1.5, so the relative intensity noise due to 1 degree of the mis-polarization can be estimated as less than 10^{-8} for the whole frequency range. The estimated intensity noise is also shown in Fig.5. The intensity noise with 1 degree of the mis-polarization is estimated under the intensity noise requirement. If we assume the thin film polarizer of the power adjustment stage in the PSL has an extinction ratio of 60 dB, this gives 1 mrad $\simeq 0.05$ degrees of mis-polarization. From these considerations, we can conclude the bow-tie cavity won't be a bad choice in terms of the mis-polarization issue.

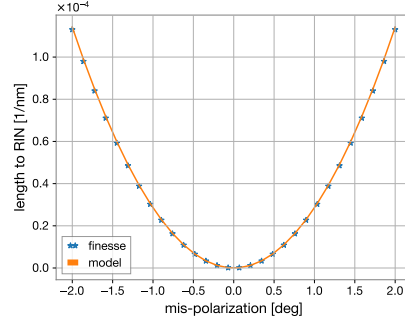


Figure 4: The calculated TF from the length fluctuation to the relative intensity noise with eq(7) and the finesse model.

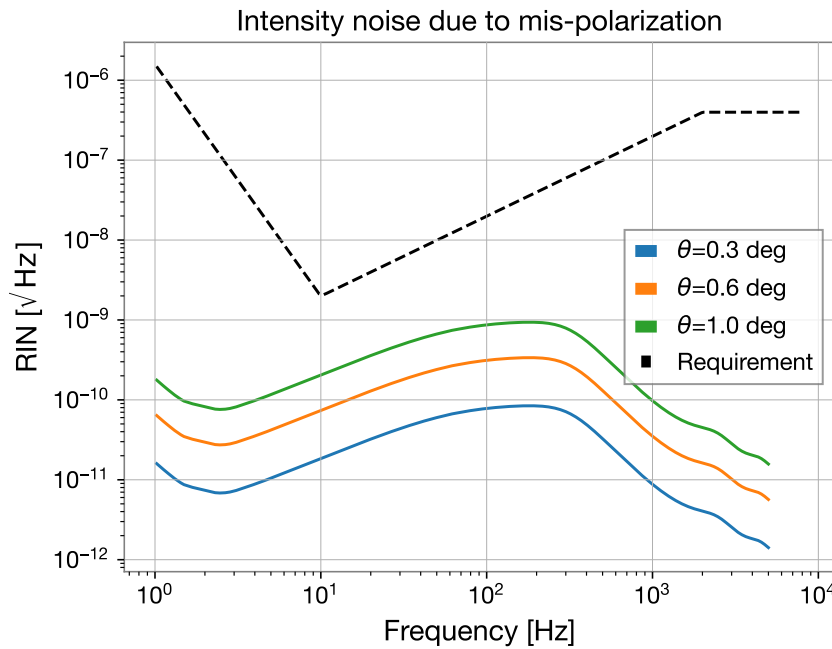


Figure 5: Relative intensity noise caused by the residual length fluctuation with mixed-polarization beam. This estimation was made with the length fluctuation calculated in Sec.???. The frequency shift is assumed as $\Delta\hat{\omega} = 0.1$.

| | Triangular | Bow Tie | Bow Tie (PMC) | |
|---------------------------------|--------------------|--------------------|--------------------|-----------------|
| Dimension | $4'' \times 0.6$ m | $4'' \times 0.5$ m | $4'' \times 0.5$ m | |
| Mirrors | 3 | 4 | 4 | |
| Mirror curvature | 5.0 | 8.5 | 3.0 | m |
| Input/output reflectivity | 2.25 | 0.98 | 2.48 | % |
| Finesse | 137 | 318 | 125 | |
| Round-trip length | 1.31 | 2.02 | 2.02 | m |
| FSR | 230 | 148 | 148 | MHz |
| Waist size (x/y) | 755/756 | 799/802 | 546/549 | μm |
| Rayleigh range (x/y) | 1.68/1.69 | 1.89/1.90 | 0.881/0.890 | m |
| Divergence angle (x/y) | 449/448 | 424/422 | 620/617 | μrad |
| Round-trip Gouy phase (x/y) | 222/42.2 | 57.0/56.8 | 101/100 | deg |
| TEM10 (hor) attenuation | 1.22 | 1.03 | 1.63 | % |
| TEM01 (ver) attenuation | 3.16 | 0.98 | 1.64 | % |

Table 1: Cavity parameters

3.2.3 RF filtering

TBD

3.2.4 Higher-order mode filtering

TBD

3.3 Conclusion

While the triangular cavity offers an advantage in addressing polarization issues, the resulting intensity noise is not expected to pose a significant problem. Moreover, using the same design as the current PMC avoids the need for designing a new cavity from scratch, saving both design effort and lead time. Since we already have spare PMCs, these can be used while new spares are being built. The attenuation gain can be improved by replacing the PMC mirrors; however, the improvement is only about 10 dB, and even with the current PMC, jitter can be reduced to a level that ensures the A+ target sensitivity with a safety factor of 10. Therefore, we propose to use the exact same design as the current PMC.

3.4 Specification of the aLIGO PMC

4 HAM1 layout

4.1 Overview

The HAM1 layout is shown in Fig. 6. The input and output periscope is used for the height adjustment between the beam height from the PSL and the ISI optical table height. The periscope has the same design as the one used in the HAM2 before the input mode cleaner(IMC). The angular actuators for the JAC and IMC alignment are the tip-tilt suspensions (JM1, JM2, and JM3). The reflection beam from JAC (JAC_REFL) is directed out to the ISCT1. The new in-vac EOM is located after the JAC. Three modematching lenses are used for the IMC mode matching. One of the leakage light from the JAC is injected to the DC PD for transmission power monitoring.

4.2 Seismic Isolation

The seismic motion will introduce jitter noise on the output mirror. The introduced jitter noise is calculated for both the ISI which is planned to be installed into HAM1 chamber and the current HAM1 table. Current HAM1 table has three stages stack for the seismic isolation.

The table motion of the HAM1-ISI is assumed to be the same as the HAM2-ISI [?]. The table motion of the HAM1 stack is based on measured values [?] below 20 Hz for horizontal motion and 100 Hz for vertical motion. Above these frequencies, a $1/f^6$ curve is assumed. These motions are illustrated in Fig. 8. While the stack provides better isolation at high frequencies, the ISI offers superior isolation below 20 Hz for horizontal motion and below 100 Hz for vertical motion.

For the output jitter noise calculation, the JAC design is assumed to be the same as the PMC. The expected output jitter noise for each table configuration is shown in Fig. 9. At frequencies where the stack has better attenuation, the residual jitter becomes dominant. Around 10 Hz, the introduced jitter noise is at a level similar to current values. The jitter noise projection is depicted in Fig. 10. The stack results in larger jitter noise below 30 Hz, and it can even approach the A+ target sensitivity.

From the perspective of seismic isolation performance, achieving the A+ sensitivity across all frequencies, particularly at low frequencies, requires the isolation performance provided by the ISI.

4.3 Mode matching

The mode matching for the JAC and IMC is designed under the following condition:

- Mode matching to JAC is done in the PSL

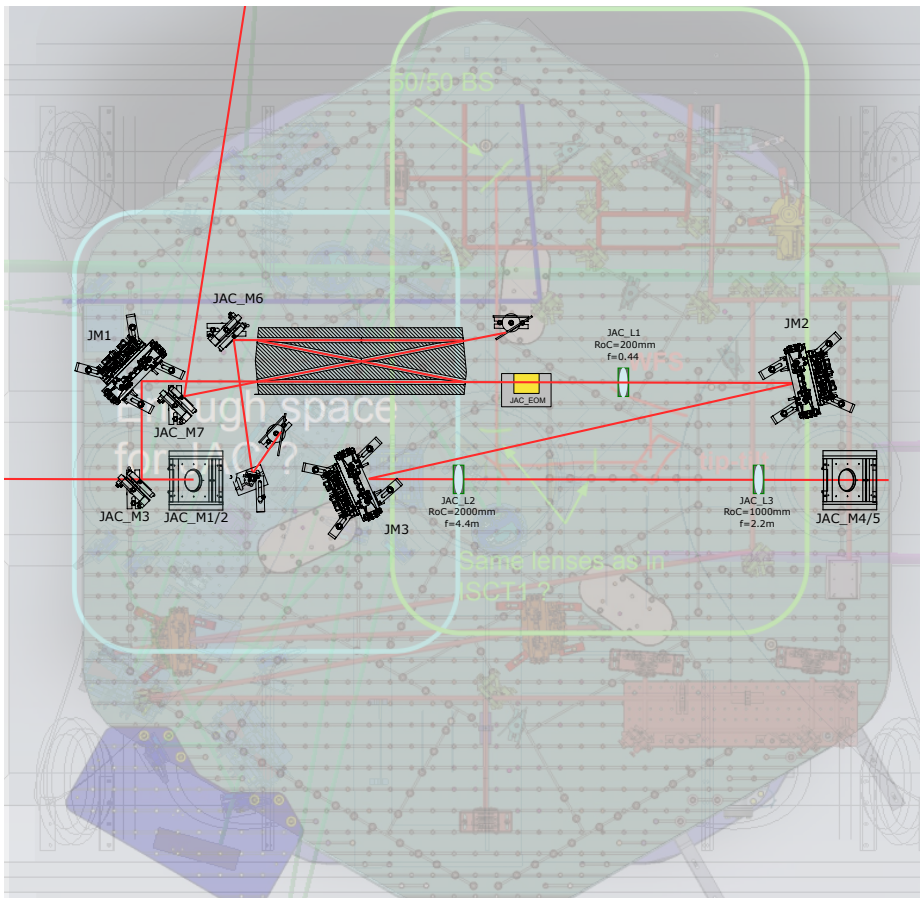


Figure 6: HAM1 layout design. The main components in the HAM1 are the JAC, three tip-tilt steering mirrors, two periscopes, an EOM.

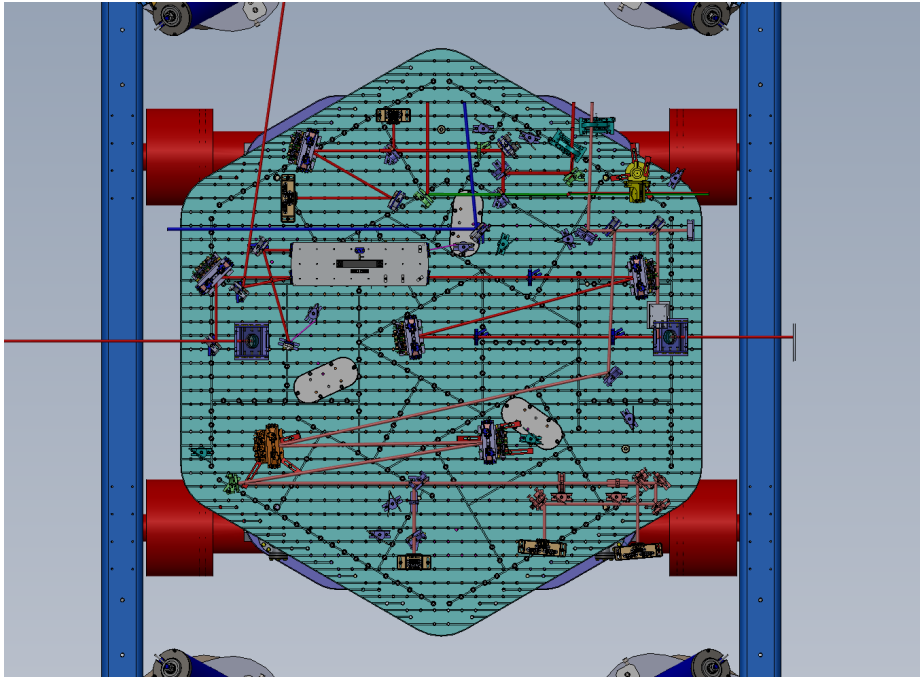


Figure 7: HAM1 layout design with other path.

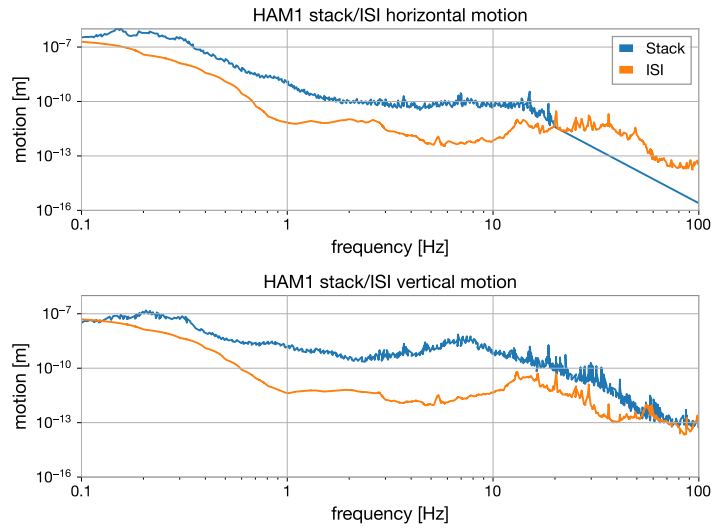


Figure 8: Caption

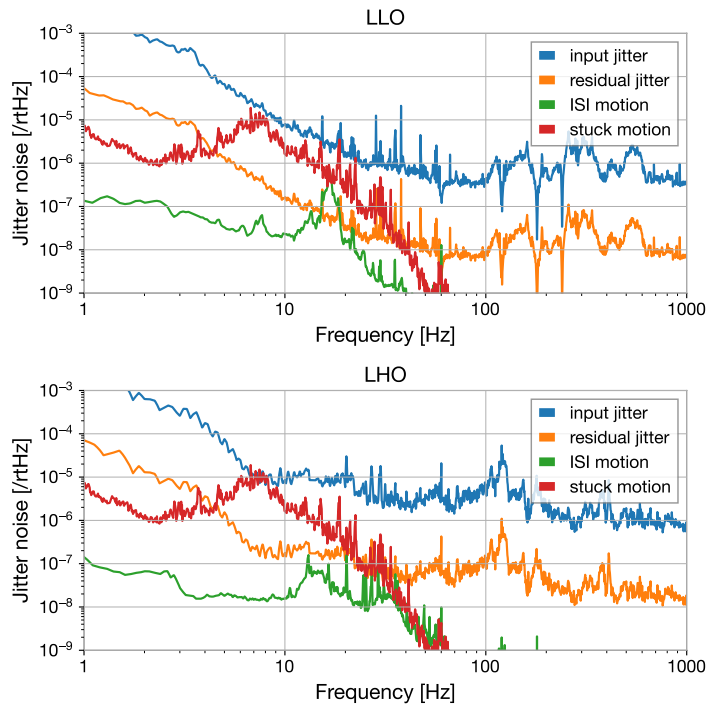


Figure 9: Expected jitter noise of the JAC output beam. Orange curve is the residual jitter of the input jitter (blue) attenuated by the JAC. Red and green are the introduced jitter by the HAM1 stack and the ISI table motion, respectively.

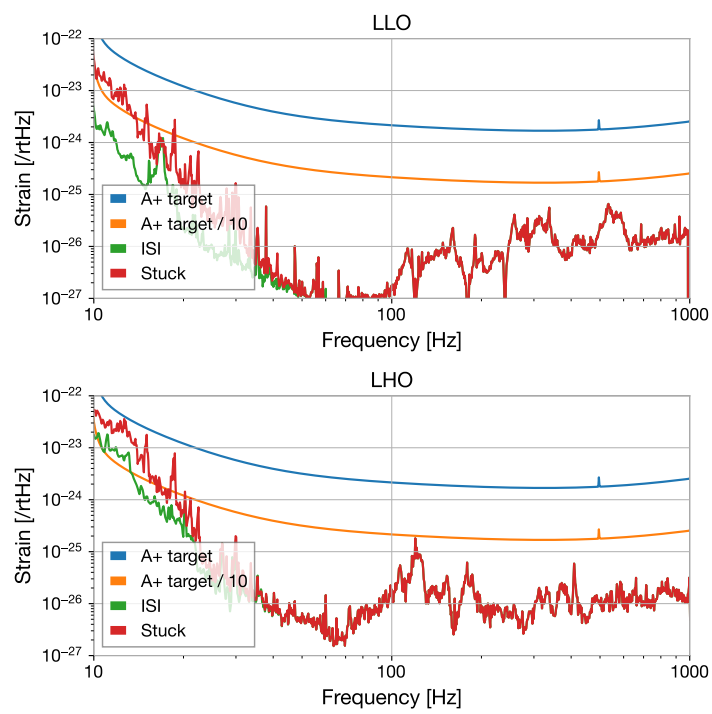


Figure 10: Expected jitter noise projection to the gravitational wave sensitivity with the ISI and HAM1-stack seismic isolation.

- Mode matching to the IMC is done in the HAM1

The distances are referred by DXXXXXXX.

4.3.1 Requirement for the mode mismatching

In the IMC REFL path, the reflected beam is attenuated by a 1000 ppm transmissive mirror and a 50/50 beam splitter before reaching the photodetector (PD). As a result, for a 100 W beam reflected from the IMC, approximately 50 mW of power is delivered to the PD.

The PD responsivity, accounting for the quantum efficiency (QE) of 0.96 and specified in the datasheet, is 0.83 A/W. Additionally, the shot noise intercept current—defined as the photocurrent at which shot noise equals the PD dark noise—is designed to be 2 mA for LSC RF photodetectors. This corresponds to an incident power of approximately 2.4 mW, which translates to a mode mismatching of 5%. Therefore, as long as the mode mismatching is below 5%, the noise contribution from the PD is dominated by its dark noise.

For the planned O5 operation, the EOM is designed to provide a modulation depth of approximately 20×10^{-3} rad. This modulation generates sidebands with a total power equivalent to about 2% of the mode mismatching. Considering this contribution, the PD noise remains dominated by its dark noise for mode mismatching up to 3%. From the perspective of IMC noise performance, setting the mode mismatching requirement to 2% appears reasonable.

In terms of power loss, the PSL itself is capable of delivering up to 110 W. To achieve the target of 100 W input to the interferometer, a mode mismatching of 2% is acceptable. Thus, this requirement balances both noise considerations and power delivery efficiency.

We don't have such strict requirement for the JAC mode-mismatching, since in any case the noise will be dominated by the JAC length motion, so we don't care so much about the PD sensing noise. But it's also reasonable to set same requirement for the JAC mode-mismatching from the view of the throughput.

4.3.2 PSL to JAC

The output beam of the PMC is injected into the EOM without any lens. This EOM is for the f1/f2 sidebands, and we are moving it into HAM1 as discussed in the following section. However, the EOM is needed here for JAC sensing, and it's preferable to maintain the current beam size on the EOM. Also, to avoid any new layout issues, we want to keep the beam path from the EOM to the PSL periscope the same as the current layout.

Thus, the first constraint for the JAC mode matching is the range where we can place the mode matching lenses. The range of the mode matching lens position is set to 4 inches after the PSL EOM and 4 inches before the bottom mirror of the PSL periscope. With the current layout, the optical path distance from the EOM to the bottom mirror of the PSL periscope is about 2.2 m, so this defines the allowable range for the lenses.

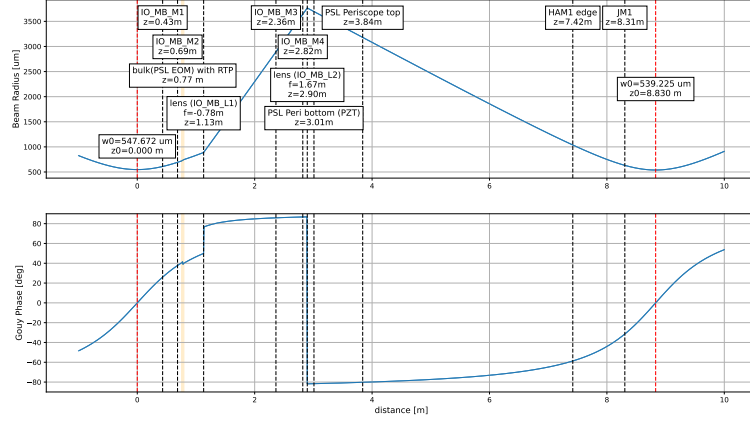


Figure 11: Beam propagation from the PSL to JAC. The first waist is that of the PMC. IO_MB_MX are the mirrors on the PSL shown in the layout figure [?]. Two mode matching lenses are located between the EOM and the PSL periscope.

The next constraint is the JAC position. The PSL periscope height is 830 mm, and the distance from the PSL periscope to the HAM1 center is 4.5 m. Assuming we place the JAC on the ISI, and considering the ISI width of 1.93 m, the distance from the PSL periscope to the HAM1 ISI edge will be approximately 3.57 m. I set the acceptable optical path length on the ISI from the edge to the JAC waist to be between 0.9 m and 1.4 m, including the periscope to kick down the beam from the PSL output to the table beam height by 0.22 m.

The mode matching solutions within these constraints are shown in Fig. 11. The solution includes two mode matching lenses: IO_MB_L1 and IO_MB_L2, with focal lengths of -0.78 m (concave: RoC of -0.35 m) and 1.67 m (convex: RoC of 0.75 m), respectively. These lenses are placed 1.13 m and 2.90 m from the PMC waist position. The layout is detailed in LIGO-DXXXXXX [?]. Fig. 12 shows how the mode changes when there is an error in the location of the lenses. The plot on the far right shows that the tolerance for the lens position to achieve 2% mode mismatching is about 1 inch. IO_MB_L2 has relatively high sensitivity to the waist size compared to IO_MB_L1. Additionally, the waist position is more sensitive than the waist size, but the waist position can also be adjusted by moving the HAM1 periscope. Therefore, we propose using IO_MB_L1 for waist size adjustment and the HAM1 periscope for waist position adjustment.

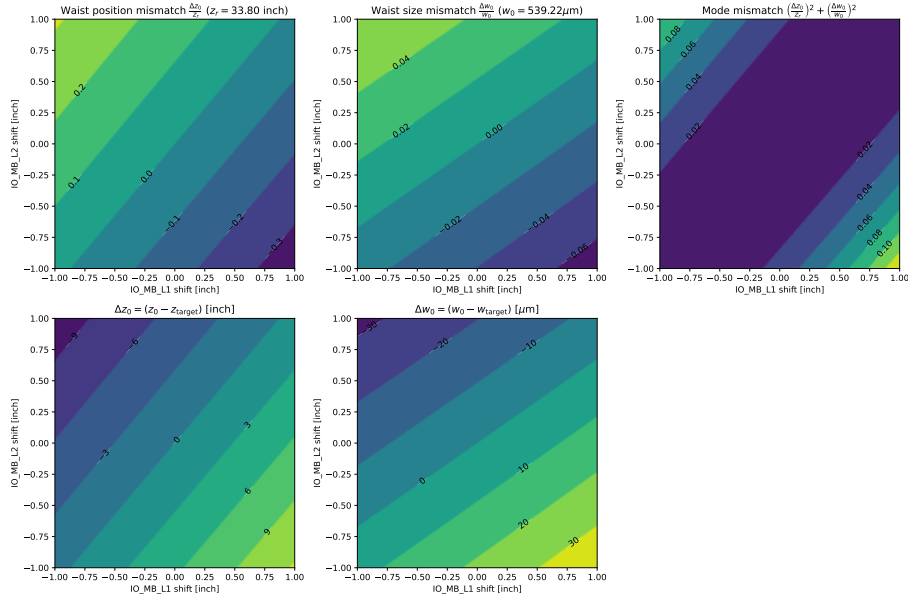


Figure 12: Contour map showing mode mismatch against the mode-matching lens position. Each plot shows the contour map for different lens positions. The horizontal and vertical axes represent the positions of IO_MB_L1 and IO_MB_L2, respectively. Each column shows the waist position error, waist size error, and total mode mismatch, respectively. The top row shows the plots with normalized error, and the bottom shows the absolute values.

4.3.3 JAC to IMC

The mode matching between the JAC and IMC will be performed on the HAM1 ISI table. An in-vacuum EOM providing the f1/f2 sidebands for the IFO LSC will replace the EOM in the PSL. Two steering mirrors will be placed between the JAC and the IMC to create a zig-zag path, allowing for path length adjustments. The center-to-center distance between the two chambers is 2570 mm, and the ISI table width is 1930 mm, leaving an edge-to-edge distance of 640 mm between HAM1 and HAM2. The beam path on HAM2 is fixed, and the distance from the HAM2 edge to the IMC waist position (located outside the IMC) is 1420 mm. A zig-zag path on HAM1 allows for a path length of approximately 3 meters, forming the first constraint for the mode matching solution.

Another constraint arises from the IMC ASC. Since there are no angular actuators in HAM2, it is beneficial to have a good Gouy phase telescope for ASC actuation in HAM1, along with the mode matching telescope for the IMC.

Considering these constraints, the proposed mode matching solution is shown in Fig. 13. The first lens (JAC_L1) is placed after the EOM to focus the beam near the first steering mirror (JM2). This configuration provides a Gouy phase separation of about 100 degrees between JM2 and JM3. JAC_L1 is placed 0.38 m from the JAC output mirror, with a focal length and RoC of 0.44 m and 0.25 m, respectively. Two lenses (RoC of 2 m and 1 m) are then positioned between JM3 and the output periscope to complete the mode matching telescope.

The mode mismatch contour maps based on the lens position are shown in Figs. 14 and 15. The advantage of this solution is that the waist size is relatively insensitive to lens position changes. Even with a 1-inch shift, the waist size only changes by 80 μm , which is 4% of the IMC waist size and results in only 0.16% mode mismatch. The waist position, however, is more sensitive than the waist size, but despite this, the tolerance for lens positioning to achieve 2% mode matching is about 2 inches.

4.4 Thermal Lens of the EOM

Since the power on the EOM will vary from 1 W to full power during the lock acquisition, the mode shape incident on the IMC will change due to the thermal lensing of the EOM. To estimate this effect, the thermal lensing effect was tested for three samples of the RTP crystal [?].

Figure 16 shows the dependence of the IMC mode mismatching on the injection power. This calculation was performed under the condition of no optimization for each sample, with the samples placed at the same position. Therefore, the optimal power is different for each sample in this scenario due to different thermal lensing effect on each crystals. The plot demonstrates that, once reasonable mode matching is achieved at low power, the deterioration in mode matching remains below 1% across the 0–100 W power variation. This suggests that the EOM thermal lensing effect is not a critical issue for IMC mode matching degradation.

It is worth noting that there was a consideration to add a translation stage

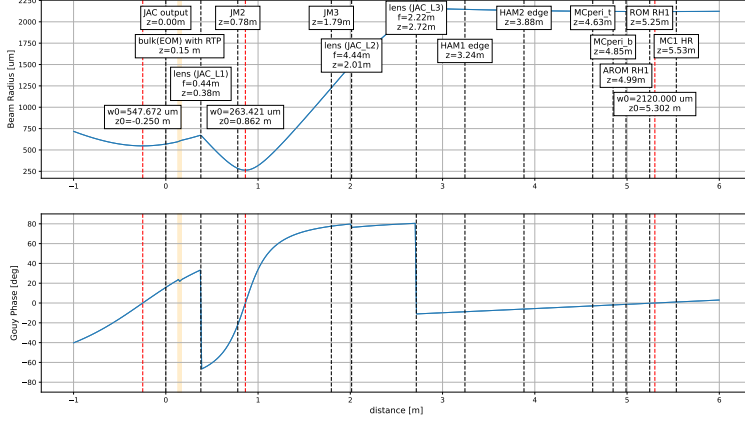


Figure 13: Beam propagation from the JAC to IMC. The first waist describes the JAC's waist. Three lenses are used for the IMC mode matching. Two tip-tilt mirrors will be used for the IMC alignment control with the gouy phase separation of 100 degrees.

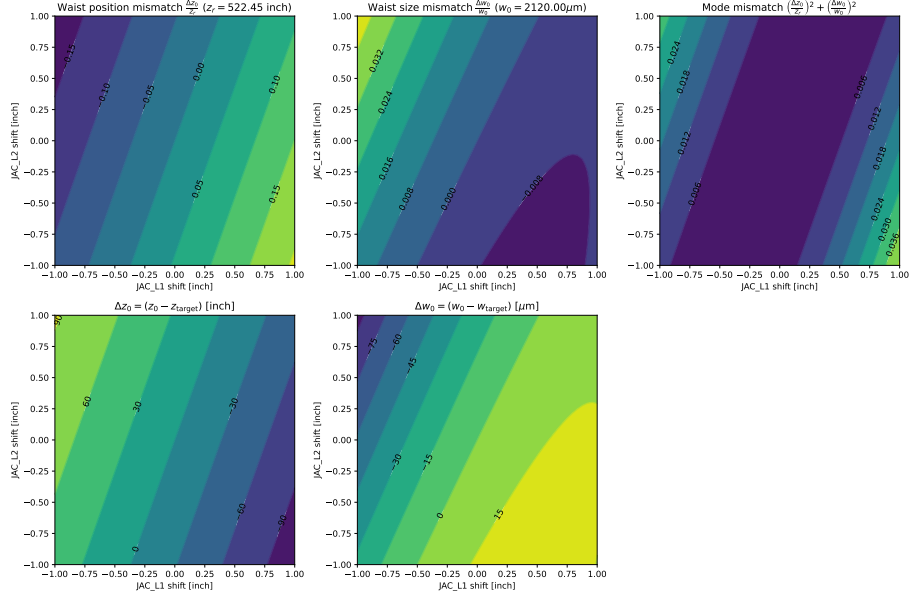


Figure 14: Contour map showing mode mismatch against the mode-matching lens position. Each plot shows the contour map for different lens positions. The horizontal and vertical axes represent the positions of JAC_L1 and JAC_L2, respectively.

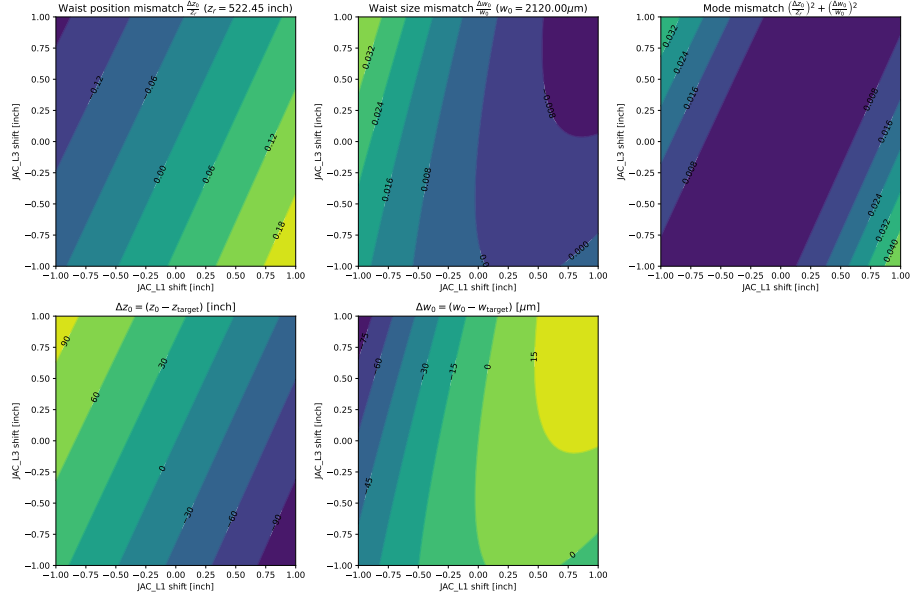


Figure 15: Contour map showing mode mismatch against the mode-matching lens position. Each plot shows the contour map for different lens positions. The horizontal and vertical axes represent the positions of JAC_L1 and JAC_L3, respectively.

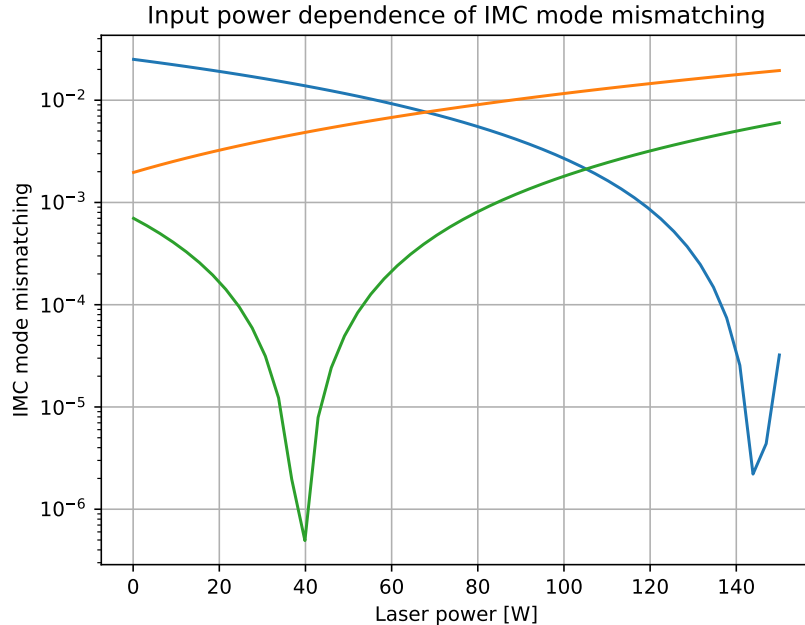


Figure 16: IMC mode mismatching dependence on the input power. The three tested RTP crystal sample is shown in the plot.

under the lens for IMC mode matching, enabling fine adjustment of the mode matching in vacuum. However, based on these discussion, we concluded that such a lens is unnecessary under these conditions.

4.5 Height adjustment

The beam line from the PSL is currently about 9 inches higher than the surface of the ISI table, so we need to lower the beam by 5 inches at HAM1. This height is constrained by the setup in HAM2, where the input Faraday isolator (IFI) is located, requiring the beam to pass above the IFI.

The first idea for height adjustment, as shown in the proposed layout, is to use a periscope to lower the beam without changing the beam line from the PSL. This approach would require two periscopes in HAM2 for both the input and output beams, which introduces some complexity.

The second option is to lower the beam height in the PSL itself. This has the added benefit of reducing input beam jitter, as the periscope height in the PSL can also be reduced. However, this would involve drilling a new hole in the PSL enclosure, designing and manufacturing a new PSL periscope, redesigning the HAM1 flange, and reconfiguring the PSL layout.

There is another available port from the PSL to HAM1 at the table height, which is currently used for the ALS. While we could theoretically use this path, it would still require modification of the PSL layout, and the two beams would be so close that it could introduce scattering or other issues.

Given the complexity of the second and third options, we believe the first approach of using an existing periscope design in HAM2 is the best solution. In terms of beam jitter, the impact should be minimal since we already have a similar periscope in HAM2, so the introduced jitter would not differ significantly between these setups.

In conclusion, we propose using the first approach as our baseline. However, for future upgrades, it could still be beneficial to lower the periscope height in the PSL.

The periscope used in HAM2 is shown in Fig. 17. We can use the exact same design for the output periscope, but for the input periscope, a modified version is needed, as both the input and output beams are on the same side. The upper mirror will need to be flipped to create a U-turn.

4.6 Viewport

The JAC reflected beam is directed from HAM1 to ISCT1. When the JAC loses lock, the full power passes through this viewport; therefore, the viewport needs to be compatible with high power. Fig. 18 shows the HAM1 flange at the +Y side. From a layout perspective, the viewport located close to the PSL and in the lower row (A2F5) is ideal. It is also beneficial not to share this viewport with any other beam to avoid potential interference.

Requirement for this viewport is similar to the IMC REFL viewport and the injection port from the PSL to the HAM1. We propose to use the same viewport as them: [D1101000](#).

4.7 Power adjustment

During the lock acquisition, the output beam power from the PSL varies from a few watts to 100W. TBD

4.8 Leakage port

The power leaking from the ports other than the input and output couplers is designed to be sensed or dumped in vacuum. This design makes it impossible to directly detect the leakage beam with a camera. However, this is not a major issue, as we have the IMC REFL camera, which can serve this purpose.

Nevertheless, it is worth keeping in mind the possibility of directing this leakage beam out of the chamber. One potential use for this beam is in adjusting the ISS inner loop. Currently, the ISS inner loop utilizes a photodetector (PD) that monitors the leak light from the PMC. However, considering the potential for excess noise introduced by the JAC, it may be advantageous to relocate the ISS sensors to one of the JAC output beams. This adjustment could reduce

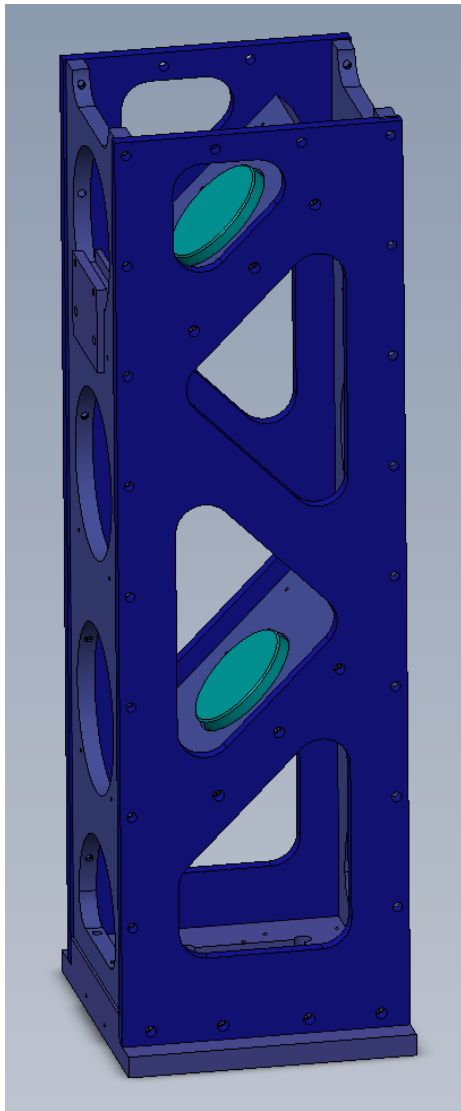


Figure 17: Periscope assembly used in HAM2 before the input mode cleaner [?]. The same design will be used for the output periscope, with a variant required for the input.

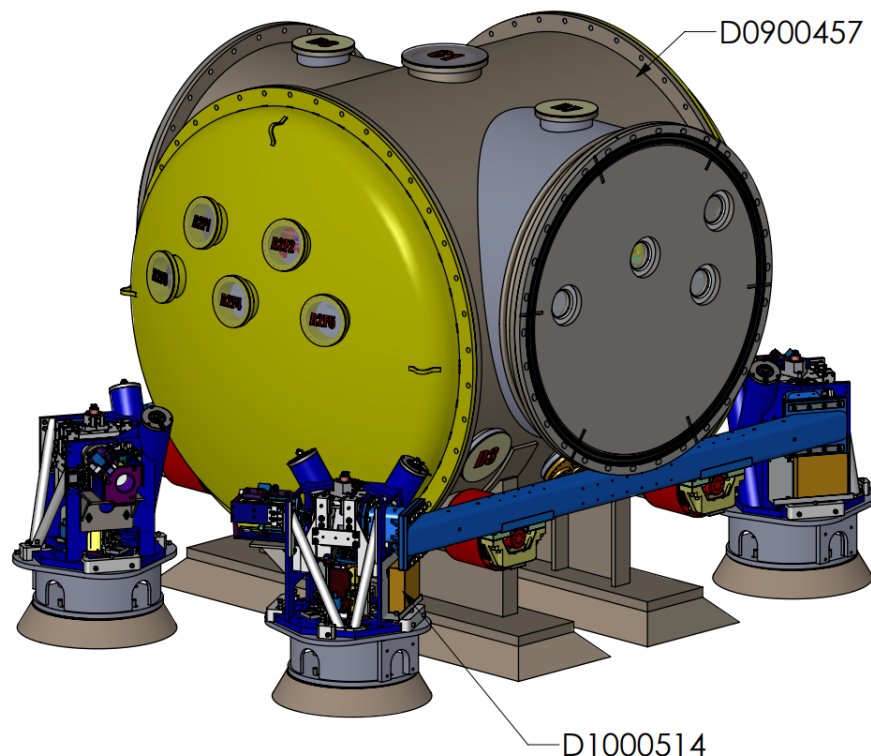


Figure 18: HAM2 chamber. Right side in the figure is the side facing to the PSL, and left side is the side facing the in-air ISCT1 table. The view port for the JAC reflection beam is bottom right (A2F5).

noise contributions and improve overall system performance. Implementing this option would require reconsidering the ISCT1 layout and wiring to accommodate the new configuration.

A similar argument could be made for the frequency stabilization system, though this would be more complex due to the intricacy of the optical path.

5 JAC Control Loop Design

5.1 Length Control

The Pound-Drever-Hall (PDH) method will be used for length control. The IO EOM located in the PSL will be used for the modulator, and the reflection from the JAC will be directed to the ISCT1 and sense the signal with the LSC PD located on the table. The digital servo will be used for the control. For the shot noise calculation, 2% of mode-mismatching is assumed.

5.1.1 Modulation

The modulation frequency is set to 43 MHz, which is twice the modulation frequency used for the PSL FSS reference cavity (21.5 MHz). This frequency was chosen because the EOM used for modulation has a 45 MHz channel, and the modulation index at 43 MHz is relatively large, approximately 0.1 rad/V [?]. Additionally, generating the RF signal is straightforward using a frequency doubler. The RF signal for modulation is taken directly from the distributor output, with a power level of 10 dBm, resulting in a modulation index of 0.01.

5.1.2 Sensor

The PD used to obtain the signal will be the LSC RFPD[?]. The responsibility of the photodiode (Excelitas, C30642 [?]) is approximately 0.82 A/W, with a quantum efficiency (QE) of 0.96 at 1064 nm, and a transimpedance is around 200 ohms. The RF beat signal will be demodulated with LSC I/Q demodulator [?], which has the conversion gain of 22 dB Vpp/Vpp [?]. The light incident on the RFPD is attenuated by a 1000 ppm transmissive BS and a 50/50 BS. The injection power to the JAC is assumed as 100 W. The PD noise is calculated with 2 mA of shotnoise intercept current[?].

The beat signal amplitude of the reflected light can be written as

$$P(\hat{\omega}) = 4P_{DC}J_0(\beta)J_1(\beta)\frac{\hat{\omega} - \hat{\omega}_0}{1 + (\hat{\omega} - \hat{\omega}_0)^2}, \quad (8)$$

where $\hat{\omega}$ is the normalized frequency by the half-width-half-maximum (HWHM) $\hat{\omega}_c$, $\hat{\omega}_0$ is the resonant frequency, $J_n(\hat{\omega})$ is the Bessel function, and β is the modulation index. The beat signal amplitude near resonance is approximately $4P_{DC}J_0(\beta)J_1(\beta)$. Thus, including the PD and I/Q demodulator parameters, the optical gain near the resonance can be calculated as 1.78 V/HWHM. The expected error signal calculated by Finesse is shown in Fig. 19.

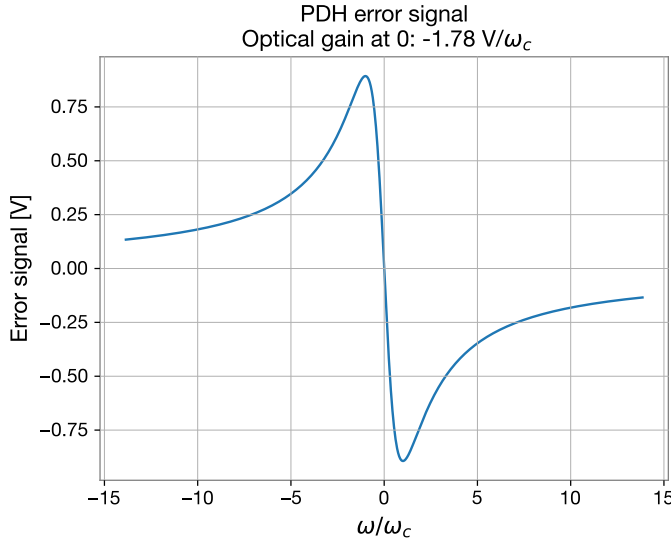


Figure 19: PDH signal at the IQ demodulator calculated by Finesse model.

5.1.3 Actuator

The actuator will use a PZT attached to the JAC. We assume the use of a Noliac NAC2125 PZT, which has a DC response of $3.3 \mu\text{m}/200\text{V}$. The high-voltage (HV) amplifier used to drive the PZT is D1001203, with a frequency response characterized by poles at 1 Hz and 500 Hz, a zero at 15 Hz, and a DC gain of 20.

5.1.4 Servo

The control system will be implemented using a digital control system of CDS. Based on the data from T2000188, the phase delay caused by the CDS is expected to be approximately 300 μsec , which corresponds to a delay of about 5 cycles at a sampling rate of 16 kHz. Since the document assumes a direct connection between the ADC and DAC, so we should consider additional phase delays caused by model dependencies. So, we assume a time delay of 500 μsec , which corresponds to approximately 8 cycles. The achievable unity gain frequency (UGF) is determined by this phase delay.

The servo will be designed with a phase margin requirement of 30 degrees. Assuming a first-order integrator and a first-order boost below 50 Hz, the open-loop gain will have a slope of $1/f^2$ below 50 Hz and $1/f$ above 50 Hz. Considering the phase response, an optimal UGF of around 200 Hz is expected. The Bode plot of the resulting open-loop transfer function is shown in Fig. 20. The phase margin is 40 degree.

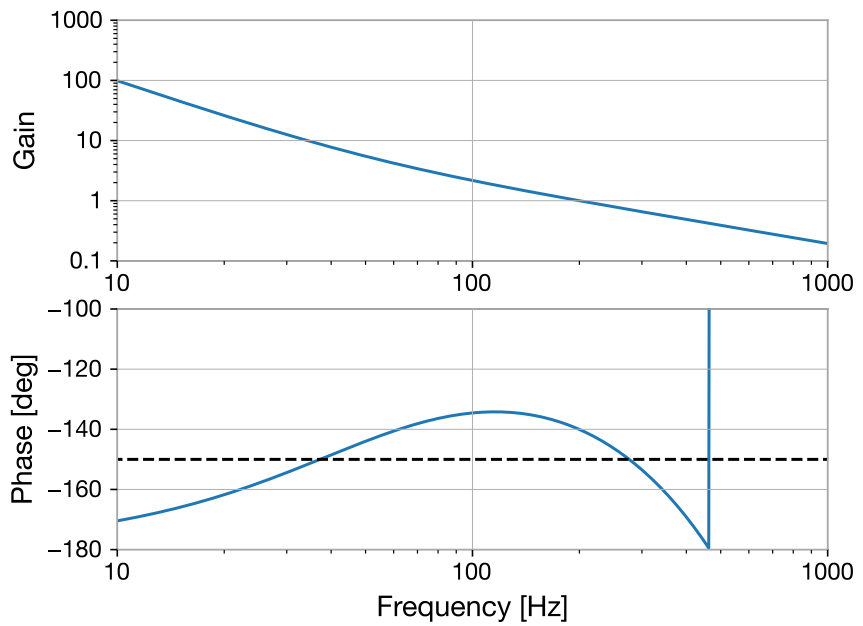


Figure 20: Open loop transfer function of the JAC LSC. Unity gain frequency is 200 Hz, and phase margin is 40 degrees.

5.1.5 Length fluctuation

The length fluctuation of the JAC was estimated based on the current length fluctuation of the PMC. Fig. 21 shows the PMC control signal multiplied by the actuator efficiency ($3.7 \mu\text{m}/1000\text{V}$). Since the PMC's length control bandwidth is in the kHz range, this serves as an estimate for the PMC's length fluctuation. However, as the JAC will be placed on the ISI and in a vacuum, this estimation overstates the length fluctuation for the JAC, particularly in the audio frequency band where acoustic noise typically dominates. Additionally, above 300 Hz, the spectrum appears to be limited by sensing or actuator noise. Therefore, we modeled the JAC's expected length fluctuation as shown by the green solid line in Fig. 21.

Fig. 22 shows the spectrum of the signal obtained from the JAC reflection sensor, including length fluctuation, shot noise, PD noise [?], and ADC noise. The ADC noise was calculated assuming two-stage whitening. The shot noise is calculated by assuming 2% of mode-mismatching, which gives about 0.9 mW DC power at the REFL PD. As shown in the figure, the signal strength is sufficient. The noise budget of the length fluctuation suppressed by the designed servo is shown in Fig. 23.

5.1.6 Intensity noise due to residual length fluctuation

To evaluate whether the suppression provided by the designed control loop is sufficient, we assess the intensity noise caused by residual length fluctuations. Same as discussed in Sec. 3.2.2, detuned cavities convert length fluctuations into intensity noise through the transfer function given by Eq. (5). The half-width-half-maximum of the JAC length variation is 2.1 nm. The previous calculation showed that length fluctuations are suppressed to below 10^{-13} m across all frequency ranges. Normalized to HWHM, this fluctuation corresponds to 4.7×10^{-5} . The intensity noise requirement for the JAC is to remain below the intensity noise stabilized by the current ISS inner loop, which is approximately 5×10^{-8} at 100 Hz as the relative intensity noise. From this, we derive that if the detuning of the cavity is less than $5.3 \times 10^{-4} \times \text{HWHM}$, or equivalently, an offset of 0.95 mV in the demodulator output, then the output intensity noise would be comparable to the current residual intensity noise of the ISS inner loop.

Fig. 24 shows the expected intensity noise caused by length fluctuation with a 1 mV and 2 mV offset, along with the inner-loop-stabilized intensity noise measured at Hanford. As shown in the figure, intensity noise remains at acceptable levels if the offset drift stays below 2 mV.

5.1.7 Phase noise due to residual length fluctuation

The residual length noise will introduce phase noise into the output beam as well. The amplitude transmissivity of the critically coupled cavity is

$$t_{\text{cav}}(\Delta \hat{L}) = \frac{1}{1 - i\Delta \hat{L}}, \quad (9)$$

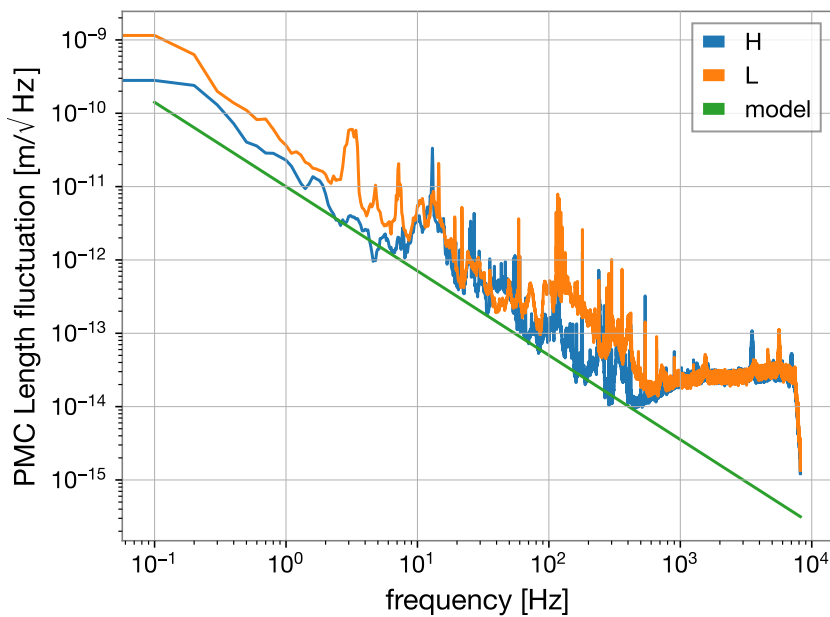


Figure 21: PMC length fluctuation of each site. This plot is using the data of L/H1:PSL-PMC_HV_MON_OUT_DQ from GPS time 1411790418 for 300 seconds. From these curves, the modeled JAC length motion is shown as solid green line.

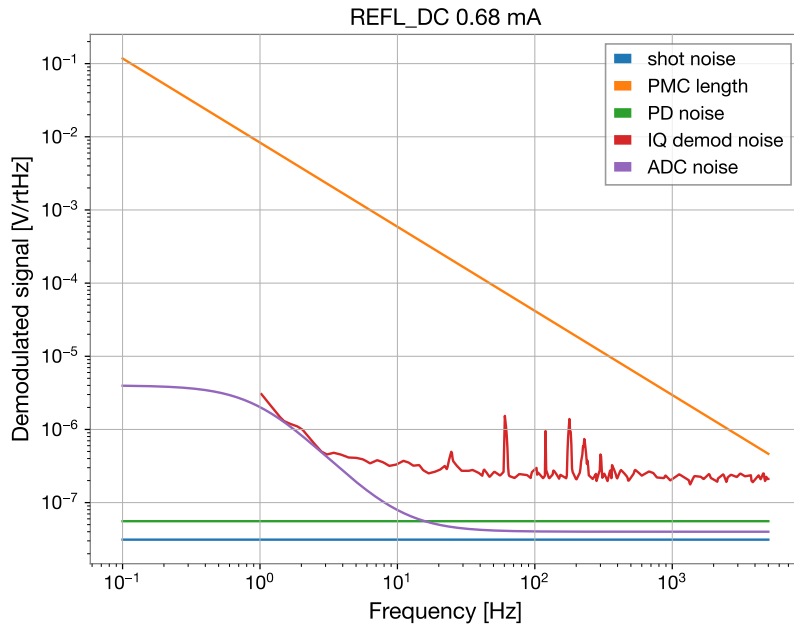


Figure 22: Expected error signal spectrum. For the shot noise calculation, 2% of mode-mismatching is assumed. The PD noise is calculated with 2 mA of shotnoise intercept current[?]. Demodulator and ADC noise refer [?], and two-stages of the whitening filter is assumed.

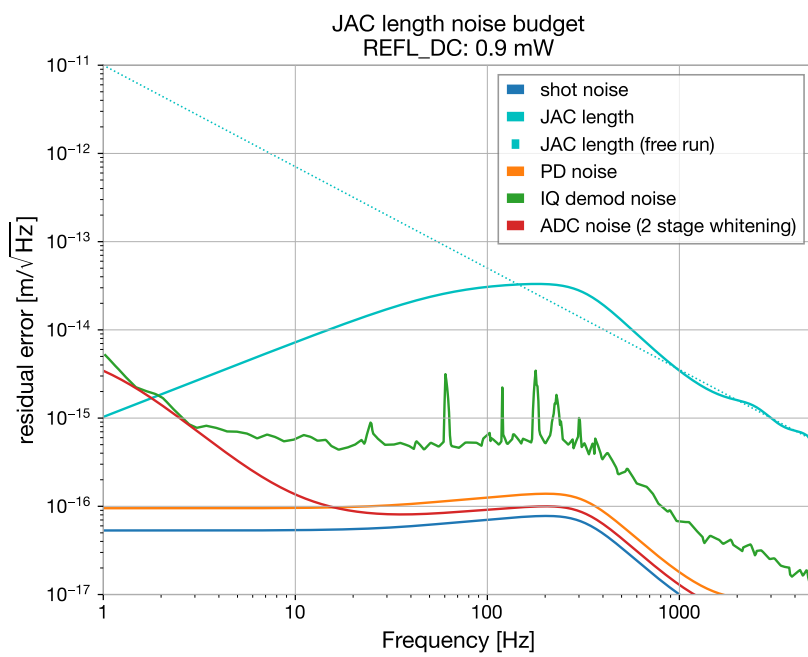


Figure 23: Noise budget of the residual length motion.

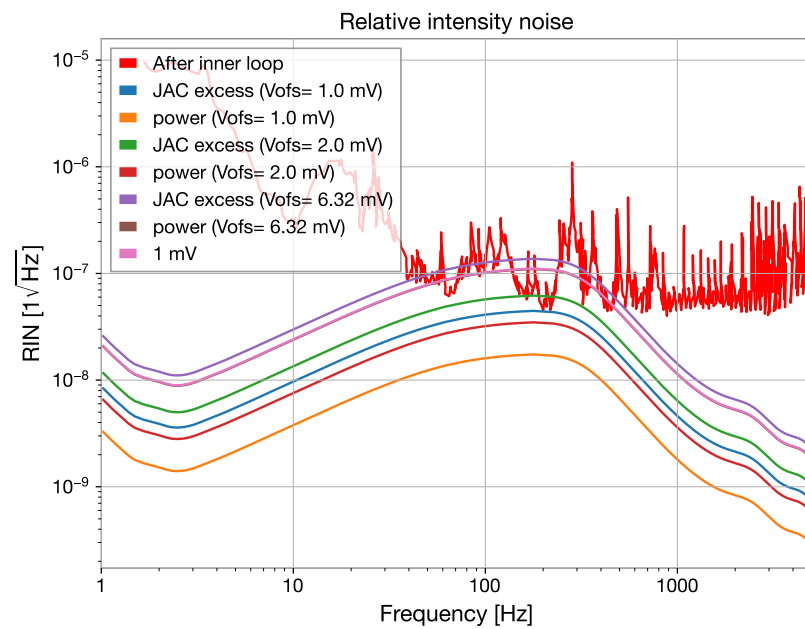


Figure 24: Expected relative intensity noise (RIN) caused by the residual JAC length motion. The current intensity noise stabilized by the ISS inner-loop is shown as red solid line [?].

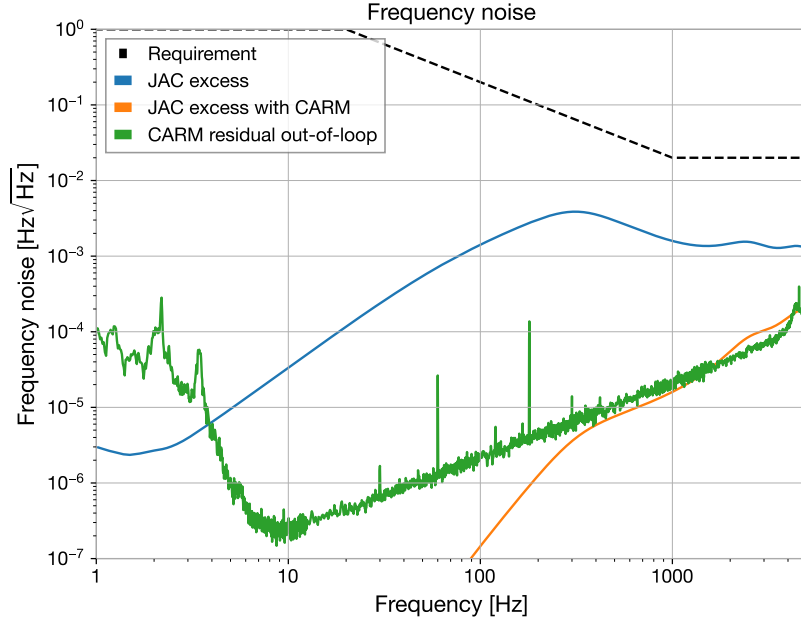


Figure 25: Frequency noise caused by the residual length noise of the JAC. The black dashed line shows the aLIGO FSS requirement [?]. Orange and green lines represent the frequency noise of the JAC output with and without the CARM loop, respectively. The CARM loop will reduce the output frequency noise to a level comparable to the current frequency noise of the input beam into the PRM.

where $\Delta\hat{L}$ is the residual length noise normalized by Half-Width-Half-Maximum (HWHM). Therefore, the phase noise of the output beam can be expressed as

$$\Delta\phi_{\text{out}} = \arctan \Delta\hat{L} \simeq \Delta\hat{L}. \quad (10)$$

A residual length fluctuation of 10^{-13} m will be converted into 4.7×10^{-5} rad of phase noise, which is equivalent to 4.7×10^{-3} Hz of frequency noise at 1 kHz.

Fig. 25 shows the estimated frequency noise caused by the residual length fluctuation of the JAC. The frequency noise will be suppressed by the CARM loop, and the suppressed frequency noise due to the JAC motion is also illustrated. This shows that the resulting frequency noise will be comparable to the current CARM residual noise.

5.1.8 Slow control

The JAC has two heaters of IS250C50RKE OHMITE. The slow drift of the cavity length (less than 0.1 Hz) will be offloaded to the JAC heater. During

the conceptual design process, heat conduction to the table was considered as a potential issue, but we believe this will not pose a problem. The heater will maintain the JAC temperature, compensating for heating by the full laser power during lock acquisition. The expected use of the heater is as follows:

1. Lock the JAC with PZT at low power (about 1 W), and offload the DC control to the heater to keep the PZT input constant.
2. During lock acquisition, maintain this slow loop. As the heat from the laser increases with more input power, this loop will keep the JAC length stable by reducing the heater output.

As a result, the total heat on the JAC will remain constant during the lock acquisition. This control scheme allows the JAC heater to prevent changes in heat conduction to the ISI table.

5.1.9 Conclusion of the length control

For the length control, our design will include the following:

- Digital control.
- Bandwidth of 200 Hz.
- Required offset drift at I/Q demodulator less than 2 mV.
- 50 mW of power will be injected into the RF PD.
- The resulting equivalent intensity and frequency noise will be comparable to the current PSL output beam.

5.2 Alignment control

TBD

6 In air table layout

The reflected beam from the JAC is directed to the ISCT1 table. The main components are the RFPD for length control and the WFSs for angular control. Additionally, a high-power beam dump is required. With this proposed layout, no changes are needed to the other REFL, POP, and ALS paths.

6.1 Layout

The ISCT1 layout design is shown in Fig. 26. The beam from the JAC reflection is directed downward by the periscope. The same periscope used for the ALS path will be utilized here. A picture and figure are shown in Fig. 28.

The first lens (JACR_L1) focuses the beam 0.7 m away from the lens with a beam radius of 625 μm . The transmissivity of the first BS (JACR_BS1) is

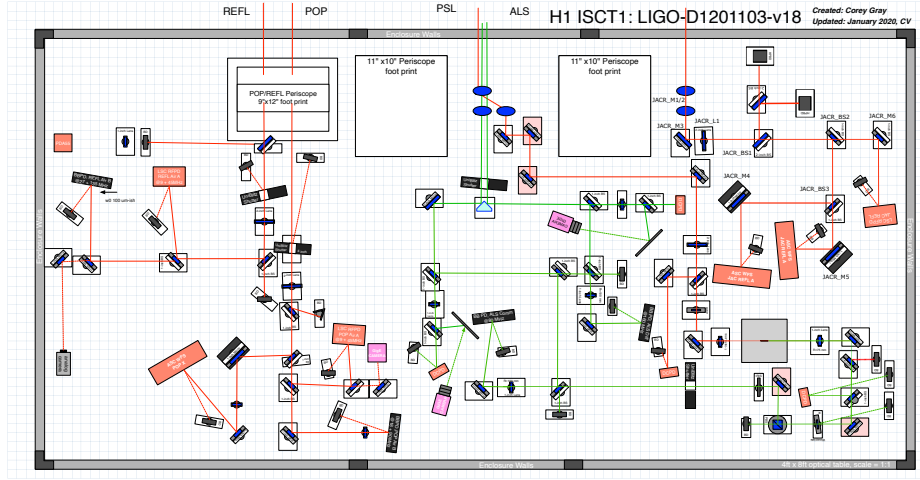


Figure 26: ISCT1 layout. The JAC reflected beam comes from the top right and is directed down by the third periscope.

designed to be 1000 ppm, so it reflects most of the power to two beam dumps, as described in the following section. The second and third BSs are 50/50 BSs to split the power between the RFPD and WFSs for JAC length and angular control. Pico-motorized steering mirrors are located for the JAC WFSs to center the DC beam position on the WFSs.

6.2 Gouy phase telescope

The Gouy phase on the WFSs is optimized by the first lens. The beam propagation is shown in Fig. 27. The Gouy phase separation for the two WFSs is 90 degrees. Note that the distance between the chamber and the table is not measured but assumed, and there might be an error in the waist position. We will need to measure the beam propagation in-situ and may need to adjust the lens position.

6.3 High power beam dump

The beam dump needs to handle over 100 W of power. While there are several water-cooled beam dump options that can handle 100 W, we currently only have an 80 W-capable beam dump cooled with a heat sink. For the O5 upgrade, the plan is to use two 80 W beam dumps for the JAC. As a future upgrade, we should keep in mind the option to replace them with a water-cooled beam dump to handle more power with a single unit.

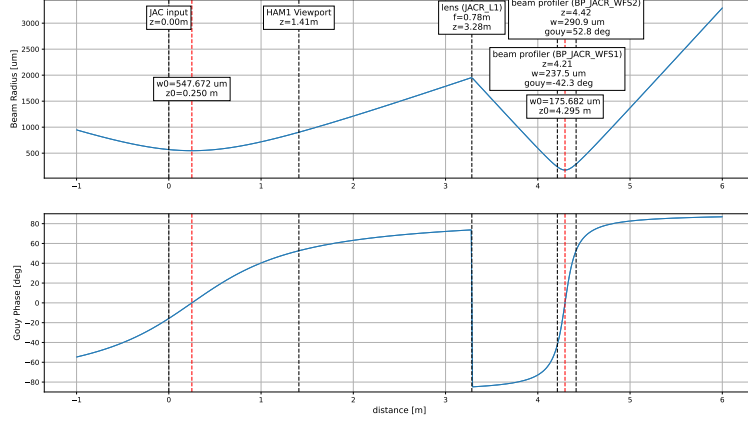


Figure 27: Beam propagation of the JAC reflection beam. JACR_L1 focuses and positions the beam waist between two WFSs.

6.4 ALS Path

To ensure safety during installation work, the ALS path has been modified without changing its length. The ALS and JAC paths are well sectioned, and no beams overlap.

7 Risk Registry

7.1 JM misalignment

When the tip-tilt suspensions (JMs) are accidentally misaligned, the full-power beam may swing inside the chamber. If the motion is too large, the beam could hit and potentially damage in-chamber components. To evaluate this risk, the beam position motion at each optic as a function of JM misalignment is calculated.

The beam position motion can be described by the following equation:

$$\begin{pmatrix} x_{\text{out}} \\ \theta_{\text{out}} \end{pmatrix} = ABCD \begin{pmatrix} x_{\text{in}} \\ \theta_{\text{in}} \end{pmatrix} \quad (11)$$

where $ABCD$ is the ABCD matrix from the misaligned optic (acting as the motion source) to the optic of interest. Here, x and θ represent the beam position and propagation angle, while "in" and "out" indicate the moving optic and the optic of interest, respectively. Assuming the beam is centered on the misaligned optic, the beam position on the optic of interest can be calculated

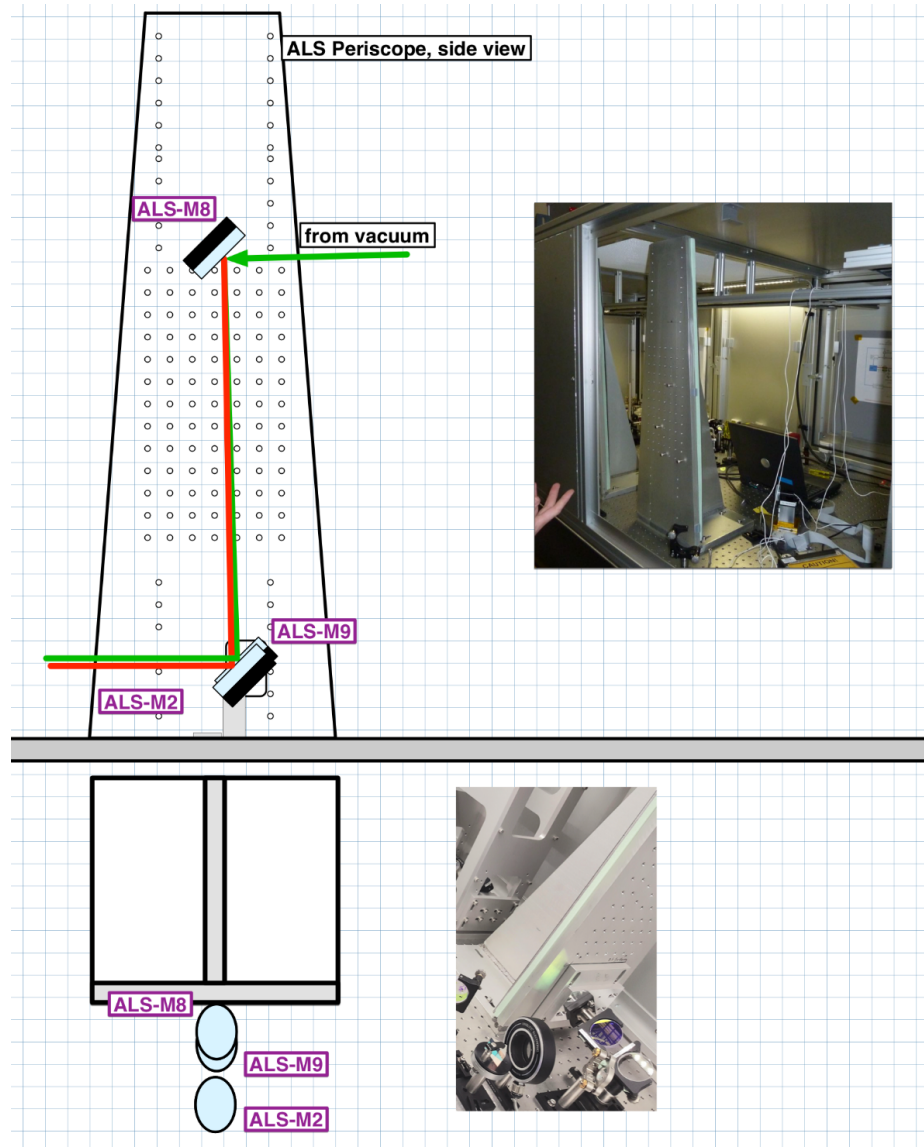


Figure 28: Periscope currently used for the ALS path on ISCT1.

as:

$$x_{\text{out}} = B\theta_{\text{in}}. \quad (12)$$

Thus, the maximum angle at which the beam does not deviate from the optic can be calculated as:

$$\theta_{\max} = \frac{d \cos \theta_{\text{AOI}}}{B}, \quad (13)$$

where d is the diameter of the optic and θ_{AOI} is the angle of incidence.

As long as the misalignment of the mirror does not exceed this angle for all optics along the beam path to the beam dump, the beam will enter the beam dump properly and be dumped without issue.

JM1

JM1 is located before the JAC, and the beam will be reflected by the JAC input coupler and directed to ISCT1. The first BS on the ISCT1 (JACR_BS1) reflects most of the power, and the beam is directed to the beam dumps (JACR_BD1 and BD2). Therefore, we need to consider the path from JM1 to the JACR beam dumps (BDs) when evaluating the JM1 misalignment. There is one lens along this path (JACR_L1), so the ABCD matrix will differ after JACR_L1.

Before JACR_L1, the ABCD matrix is:

$$B = L \quad (14)$$

and after JACR_L1, it will be:

$$B = \left(1 - \frac{L_f}{f}\right)L + \frac{L_f^2}{f} = (-3.3 \times L + 14.3) \quad (15)$$

where L is the distance from the misaligned optic, f is the focal length of the lens, and L_f is the distance of the lens from the misaligned optic. The distances and the maximum allowable angles are shown in Table 2. The error is caused by position uncertainty, with all optics assumed to have a position error of 5 mm. The minimum allowance is for the beam dump and 3 mrad.

| Optic Name | Distance (m) | Max Angle (degrees) |
|------------|--------------|---------------------|
| JAC input | 0.2750 | 36.11(66) |
| JAC_M2 | 0.4550 | 31.56(35) |
| JACR_M1 | 2.6850 | 5.351(11) |
| JACR_M2 | 3.2410 | 4.4341(67) |
| JACR_L1 | 3.3299 | 6.127(29) |
| JACR_M3 | 3.4315 | 4.796(42) |
| JACR_BS1 | 3.5966 | 5.862(62) |
| JACR_BS4 | 3.7744 | 7.68(10) |
| JACR_BD | 3.9268 | 3.206(55) |

Table 2: Distances and maximum allowable angles for each optic.

JM2 and JM3

The beam reflected by JM2 and JM3 directes to HAM2 and reflected by input mirror of the IMC, and directed out to IOT1. We don't have no lens between JM2 and JM3, so the maximum allowance angle is always smaller for JM2 than JM3. Thus, we only show the calculation of JM2 here.

| Optic Name | Distance from JM2 (m) | Max Angle JM2 (mrad) | Max Angle JM3 (mrad) |
|------------|-----------------------|----------------------|----------------------|
| JAC_M4 | 2.1352 | 8.315 ± 0.017 | 14.417 ± 0.048 |
| JAC_M5 | 2.3562 | 8.378 ± 0.015 | 12.847 ± 0.035 |
| MCperi_t | 3.8477 | 8.848 ± 0.012 | 7.401 ± 0.015 |
| MCperi_b | 4.0687 | 8.922 ± 0.013 | 6.964 ± 0.015 |
| AROM RH1 | 4.2087 | 10.985 ± 0.018 | 8.219 ± 0.019 |
| ROM RH1 | 4.4657 | 11.094 ± 0.020 | 7.710 ± 0.019 |
| MC1 HR | 4.7540 | 27.474 ± 0.064 | 17.656 ± 0.041 |
| MCR_Per1_b | 5.1709 | 9.310 ± 0.026 | 5.379 ± 0.013 |
| MCR_Per1_t | 5.2709 | 9.348 ± 0.026 | 5.270 ± 0.013 |
| MCR_Per2_t | 6.0209 | 9.633 ± 0.038 | 4.575 ± 0.012 |
| MCR_Per2_b | 6.1209 | 9.677 ± 0.037 | 4.496 ± 0.012 |
| MCR_M1 | 8.5949 | 10.768 ± 0.087 | 3.1497 ± 0.0100 |
| MCR_M2 | 9.1509 | 11.04 ± 0.11 | 2.9526 ± 0.0092 |
| MCR_AR1 | 9.7069 | 11.34 ± 0.12 | 2.7764 ± 0.0088 |
| MCR_M3 | 10.2629 | 11.65 ± 0.14 | 2.6219 ± 0.0087 |
| MCR_M4 | 10.8189 | 11.98 ± 0.15 | 2.4820 ± 0.0078 |
| MCR_BD1 | 11.3749 | 17.41 ± 0.24 | 3.335 ± 0.011 |
| JAC_L2 | 1.2342 | 8.238 ± 0.029 | 46.3 ± 1.1 |
| JAC_L3 | 1.9352 | 5.8445 ± 0.0100 | 11.478 ± 0.052 |

Table 3: Distances and maximum allowable angles for each optic.

8 Open questions

8.1 Thermal effect of the JAC

While the thermal lensing of the EOM has been verified to not pose a significant issue, the thermal effects of the JAC itself remain untested. As the input power changes from a few watts to over a hundred watts, the thermal conditions within the JAC will shift drastically. Although the heater will be used as part of the thermal compensation system, local thermal gradients, such as thermal lensing of the input or output mirrors and deformation of the JAC body, cannot be fully avoided. These effects may lead to changes in the output mode or alignment drift. Alignment compensation may be achievable through the tip-tilt suspensions, but if the available compensation range proves insufficient, it may be necessary to design an in-vacuum power adjustment stage.

8.2 Length fluctuation

The design calculations are based on assumed length fluctuations, estimated from the in-air PMC length fluctuations. However, it is possible that these assumptions underestimate the actual length fluctuations, leading to higher intensity and frequency noises in the output beam. During the testing phase, it will be necessary to evaluate the actual length fluctuation. If it is found to be larger than expected, we may need to increase the control bandwidth beyond the current design, potentially up to the kHz range. This could be achieved by switching from digital control to an analog servo system.

Related to the length fluctuation, the PMC is equipped with a damping structure designed to suppress body resonance. This structure utilizes Viton sheets, clamped from above, to apply force and mitigate resonant modes. It may require redesigning to improve performance and ensure compatibility with vacuum conditions.

8.3 Stray light control

The main sources of stray light are the viewport for the JAC reflection beam and the high-power beam dump located on the ISCT1 table. Assuming a few percent of mode mismatch, the power injected into these components can reach a few watts. Although the backscattered light may not directly couple with the main beam, the presence of POP and REFL PDs used for the main interferometer's ISC presents a risk. In particular, scattered light could potentially couple with DARM through auxiliary degrees of freedom.

9 Safety

9.1 Laser safety

In-chamber

For the JAC installation, alignment work can be done with a low-power laser. Before entering the chamber, ensure that the power from the PSL is sufficiently low (<100 mW).

Once the JAC is aligned and installed, a high-power test will also be required. Close all the flanges, monitor the inside of the chamber with a camera, and gradually increase the laser power.

Maintain the LVEA laser hazard status throughout the entire installation process.

ISCT1

We also need to align the ISCT1 table. As with the in-chamber work, the LVEA must be set as a laser hazard area. For the ISCT1 work, personnel must also be cautious of other beam paths, particularly the ALS-PSL path. This path is close to the JAC reflection path, and the power exceeds 1 W. Therefore, it is

recommended to conduct the work with an expert familiar with the ALS-PSL path.

10 Wiring

10.1 Analog circuit

The main circuit is the modulator and demodulator for the length and alignment sensing. These circuite will be located in PSL_R1, PSL_R2, ISC_R1, ISC_R2, ISC_R4. Also, for tip-tilt actuation, we place the coil driver on SUS_C4, and saterite box on SUS_R1. The rack layout is working in progress.

10.2 CDS

- The model will run in l/h1imc or make new model l/h1jac? -

10.3 HAM1 flange feedthrough

The main electronics in the HAM1 chamber related to the JAC will be

- 3 x Tip-tilt suspension
- JAC Controls (PZT, thermometer, and heater)
- DC PD
- EOM

Each tip-tilt needs a D25 connection for OSEM sensing and control. JAC PZT, JAC thermometer, heater, and DCPD will share a D25 cable. Therefore, four D25 connections are needed. The EOM has four electrodes, and each connection will use a coax cable.

Summarizing these cables, the required feedthroughs are:

- 2 x dual-D25: [D2000223](#)
- 1 x five-coax (Accuglass_25D-5CX-450): [D1600167](#)

11 Vacuum compatibility

11.1 Cavity

11.2 Electronics

12 Test plan

The test configuration is

12.1 Jitter attenuation

13 Installation plan

14